Scientia Iranica B (2015) 22(3), 743–754

SCIENTIA IRANICA

Sharif University of Technology
Scientia Iranica
Transactions B: Mechanical Engineering
www.scientiairanica.com

Aspects of canard-wing vortices interaction in subsonic flow

A.R. Davari[a,*], M. HadiDoolabi[b], M.R. Soltani[c] and M. Izadkhah[c]

a. *Department of Mechanical and Aerospace Engineering, Science and Research Branch, Islamic Azad University, Poonak, Tehran, I.R. Iran.*
b. *Department of Aerospace Engineering, Malek Ashtar University, Tehran, Iran.*
c. *Department of Aerospace Engineering, Sharif University of Technology, Tehran.*

Received 11 October 2012; received in revised form 10 October 2014; accepted 15 November 2014

KEYWORDS
Canard;
Vortex;
Interaction;
Burst;
Delta wing;
Tip vortex.

Abstract. A series of subsonic wind tunnel tests were conducted on a canard-wing configuration to study the interaction of canard and wing vortices. Both the canard and the wing in the present experiments had equal sweep angles. The velocity contours were measured using a total-static rake at three chordwise positions at front, middle and rear parts of the wing in a plane perpendicular to the wing surface. The experiments were performed at various combinations of attack and canard deflection angle. The results show a close relationship between the strength of the vortices and the outcome of their interaction. According to the present findings, when the wing strong vortex is exposed to the strong vortex of the canard, the result of this interaction would be a weaker vortex on the wing with a smaller size than the original two vortices, while a weak vortex on the canard interacted with a strong vortex on the wing, amplifies it and results in a stronger vortex on the wing surface. This has also been shown to be true when a strong canard vortex interacts with a weak vortex on the wing. The result would again be a stronger vortex on the wing surface.

1. Introduction

At high angles of attack, delta wings produce high lift due to the vortical flow system over their suction sides, which enable maneuvering capability at low speeds. In addition, high sweep delta wings are desirable in high speed cruise regimes. Close-coupled delta wing and canard configurations have great advantages on the wing flowfield. Canard has favorable effect on the aerodynamic characteristics of aircraft such as instantaneous pitching control, increasing maximum lift and a potential to increase lift to drag ratio and maneuverability [1].

In the late 1950's, widespread cutting-edge researches were conducted with the subject of vortical flow over delta wings. Er-El [2] carried out an extensive study on the downstream effects of the canard sweep angles and positions of the loading of a delta wing. His results showed that highly swept canard produces stronger leading edge vortices that induce lower pressure region over the wing; a result which is less evident in the moderate sweep canards.

Calarese [3] performed an experimental study to investigate the interaction of the vortices shed by canard and wing leading edges, and their effects on a close-coupled canard-wing configuration in different wind tunnels. He investigated the effects of the model size, the Mach number, the angle of attack and the

*. *Corresponding author. Tel.: +98 21 44868536*
E-mail addresses: ardavari@srbiau.ac.ir (A.R. Davari); hadidoolabi@yahoo.com (M. HadiDoolabi); msoltani@sharif.edu (M.R. Soltani); m_izadkhah@yahoo.com (M. Izadkhah)

spanwise blowing effects on the vortex interaction. According to his results, a coplanar canard produces a small favorable interaction between the leading edge vortices, while an off-set canard produced a considerable increase in the lift to drag ratio.

Rom et al. [4] conducted a series of experimental measurements on the aerodynamic characteristics of several close-coupled wing-canard configurations up to moderately high angles of attack. They compared the longitudinal aerodynamic coefficients, the rolled-up vortex trajectories, and the pressure distributions for five wing-canard configurations. They examined various canard deflections and canard positions relative to the wing. Their results indicate that a positive canard deflection causes a slight increase in the maximum lift of the configuration while having only small effect on the variation of the lift as a function of the attack angle. They also reported a decrease in the lift to drag ratio at positive canard deflections for small to moderate angles of attack.

Hummel and Oelker [5,6] performed comprehensive surface pressure measurements and flow visualizations on various lateral and longitudinal canard positions with different setting angles. In their studies, the effects of the body on the flowfield were eliminated by using a thin vertical body. From their findings, canard induces a non-uniform angle of attack distribution on the wing, which suppresses flow separation in the front parts and supports vortex shedding in the rear parts. Due to downwash effects, vortex breakdown is delayed within the wing vortex system. They also found that tendency of merging the two vortices is enhanced by increasing the angle of attack which is more evident for the mid canard configurations.

Up to 1990, the experiments were mostly concentrated on canard and wing without taking the fuselage effects into account. In 1993, Howard [7] tested a model including canard, wing and fuselage. A tertiary vortex was observed at the juncture of canard and fuselage that had an impact on the resulting flow and was not observed in the earlier researches of wing-canard combinations in the absence of body.

Bergmann and Hummel [8] examined body-wing-canard configurations in a symmetrical flow. Their results show that the effects of canard vortex on the flow over the wing are considerable for large deflections and lower canard positions, i.e. the canard surface is located much lower than the wing. However, at very low canard positions, this favorable interference effect vanishes. The vortex breakdown on the canard deteriorates the vortical flow at all angles of attack, and this leads to a considerable loss of lift.

In addition to the experimental studies, various numerical simulations have also been performed on the canard-wing configurations. Eugene [9] solved a thin-layer approximation of the Navier-Stokes equations to investigate the effects of canard vertical position on a close-coupled, canard-wing-body configuration. The computational results showed favorable canard-wing interactions for the high and mid canard positions. It was revealed that unfavorable results for the low canard configuration are directly attributed to the interaction between the canard and the wing vortices.

Ekaterinaris [10] analyzed the flowfield of a canard-wing-body configuration at subsonic speeds and at high angle of attack by a Navier-Stokes flow solver with overset grids. He predicted vortex breakdown as well as its delay due to the canard influence.

Tuncer and Platzer [11] investigated the subsonic flowfield over a close-coupled delta canard-wing-body configuration at high angles of attack using a Navier-Stokes solver. They presented their results in terms of particle traces, surface streamlines and leeward-side surface pressure distributions for both canard-on and canard-off configurations. They found that the presence of canard delays wing vortex breakdown to positions aft of the wing trailing edge.

In recent years, the studies on the aerodynamics of canard-wing body configurations, has mainly been concentrated on the vortical flow control over the lifting surfaces. Canard flow controlled by spanwise pulsed blowing has been found to play an important role in increasing the aerodynamic performance of canard-wing body configurations, especially in the circumstances when an indirect wing flow control is desired [12,13].

Cui et al. [14,15] successfully examined forebody slot blowing to postpone the vortex break down onset on a delta wing. They also found that a symmetric blowing on both the upper and the lower surfaces leads to the best performance. To develop a concept to be used as an active flow control actuator for a delta wing, Chung et al. [16] studied the interaction and merging processes of the co-rotating and counter rotating vortex pairs generated in a strake-delta wing configuration, as well as their impact on aerodynamic forces through CFD simulations. They observed that a counter-rotating vortex pair at high angles of attack has a pronounced effect on the overall vortex system and consequently on aerodynamic forces of the delta wing.

Nearly all studies undertaken so far, were concentrated on the canard effects on the forces and moments of the aircraft or the canard signature on the flow field over the wing. Though valuable information has already been obtained on the effects of canard on the flowfield over the wing, to the authors' knowledge, none was reported to deal with the physical interpretation of the canard-wing vortices interaction and their merge.

In the present research, effects of canard on the wing flowfield were investigated for a canard-wing-body configuration. The results include the velocity field at three chordwise planes normal to the wing

surface. For various combinations of angle of attack and canard deflection angle, the effects of canard vortex were studied on the wing flowfield. This study revealed the interaction law of canard-wing vortices. The results can be thought of as a different view point to the vortex interaction phenomenon. The conditions under which the wing vortex is amplified or attenuated by the canard flow are examined and addressed in the paper. These findings can be extensively used in nearly all canard-wing flying vehicles at moderate to high angles of attack.

2. Experimental setup and procedure

The experiments were carried out in a subsonic closed circuit wind tunnel with test section dimensions of 0.8 m×0.8 m. The maximum attainable speed at the test section is 100 m/sec. Using hot wire anemometry the turbulence intensity at the test section was measured to be less than about 0.1%.

The model considered in the present experiments was a close coupled wing-canard configuration attached on a half body. Figure 1 shows the model installed in the test section along with the rake probes used for the velocity measurements. Both the wing and the canard had a flat platform with sharp leading edges.

The wing and the canard were attached on the fuselage in such a way that the wing apex was very close to the canard trailing edge. Table 1 summarizes the geometric characteristics of both planforms.

The velocity field in a plane perpendicular to the wing surface at three chordwise locations ($x/c = 0.44$ at the front part, $x/c = 0.69$ at the middle and $x/c = 1.00$ at the rear of the wing) at different combinations

Figure 1. The model installed in the test section with the rake probes behind.

Table 1. Geometric parameters of the model planforms.

	Wing	Canard
Leading edge sweep angle	60°	60°
Span to chord ratio	0.56	0.62
Thickness to root chord ratio	0.02	0.03
Leading edge bevel angle	15°	15°

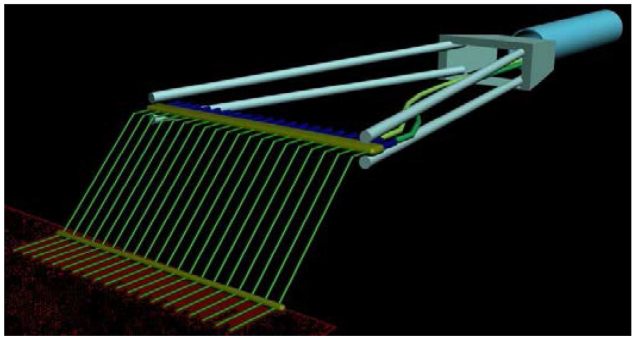

Figure 2. Schematic of the rake designed for the present experiments.

of model angle of attack and canard deflection angle was measured. The corresponding canard-off tests on the wing alone configuration were also carried out as well.

The experiments were conducted at a single Reynolds number of 0.825×10^6 based on the wing root chord. The angles of attack were varied from 0° to 25° with an increment of 5°. The canard deflection angles were measured with respect to the body and ranged from -10° to 10°.

The rake used for the measurements was especially designed to impart as minimum disturbance in the field as possible and was more slender than the conventional rakes. Figure 2 shows a schematic view of the rake manufactured and used in the present experiments. The rake had 10 total pressure and 10 static pressure tubes, which were 10 mm apart. The internal diameter of the tubes was 0.9 mm. Two 45° bends were provided in the tubes to reduce the interference effects of the supporting system at the position under measurement. The model maximum blockage ratio including wing and canard planform areas was measured to be less than %5.

Due to some restrictions during the test, the rake could not be traversed spanwise in the test section to cover the entire wing span. To retrieve the information regarding the flowfield lost by these restrictions, a numerical simulation was also performed over the configuration.

The probes were connected by short plastic tubes to high frequency pressure sensors with 30 kHz acquisition rate and ±5 psi measuring range located outside the test section. Different tube lengths and materials were examined to find the best choice to reduce the associated losses and time lags.

A high frequency data acquisition system was employed to acquire the data. The acquisition rate was 100 samples per second and the data presented in this paper is an average of 3000 samples for each channel of the A/D board. Total errors encountered by the measured data including the accuracy of the electronic devices such as transducers and acquisition

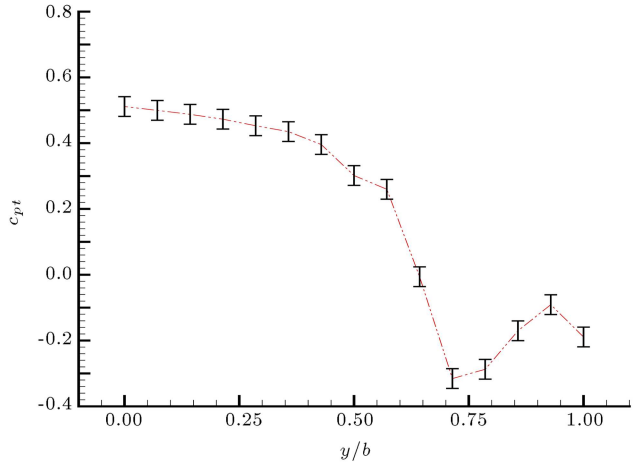

Figure 3. Typical data uncertainty.

board were estimated to be less than ±3%. Figure 3 shows a typical data uncertainty analysis on the total pressure measurements.

3. The numerical survey

As stated earlier, since the rake provided for the present experiments was not wide enough to scan the entire wing span, nor was possible a spanwise traversing of the rake on the wing, only the outboard region of the wing was captured by the rake. To achieve a better insight through the flowfield over the entire model, a numerical analysis was carried out on this configuration.

The equation used for the numerical simulations in the present work was the full Navier-Stokes equation for viscous flow which has been discritized on unstructured grids and solved by a commercial code. Since the flow regime was incompressible, the pressure based algorithm was used to solve the equations. To take the simultaneous advantages of $k\omega$ near the wall and $k-\varepsilon$ for farfield, the k-ω-SST turbulence model was used. This model also seems to be a suitable choice to take the flow transition effects into account.

The flow inlet and outlet were considered on a sphere having a radius of 20 times the body length and only half of the model was analyzed owing to symmetry of the problem. The boundary layer mesh was used for near body regions and for the rest of the field, tetragonal and pentagonal cells were generated. The cell distributions on a longitudinal cross section are shown in Figure 4.

To check the grid independency, 1.0, 1.5 and 2 million cells, i.e. coarse, medium and fine grids, were considered and the same results with a good accuracy were achieved for the two later cases. On this basis 1.5 million cells were chosen for the rest of the analysis. Figure 5 shows the associated results for the model considered in the present experiments.

The Hummel's canard-wing model [17] was first

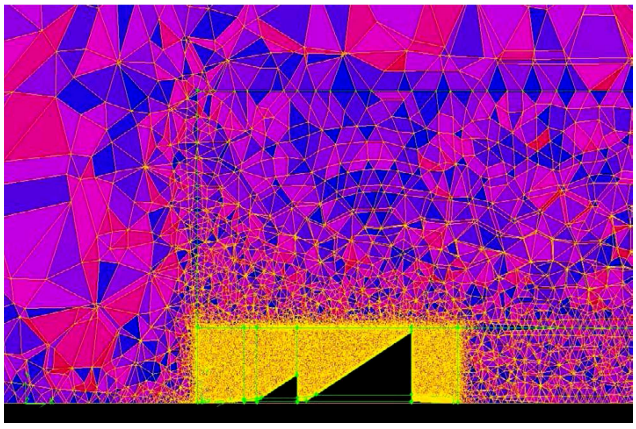

Figure 4. The cell distribution at a longitudinal section of the field.

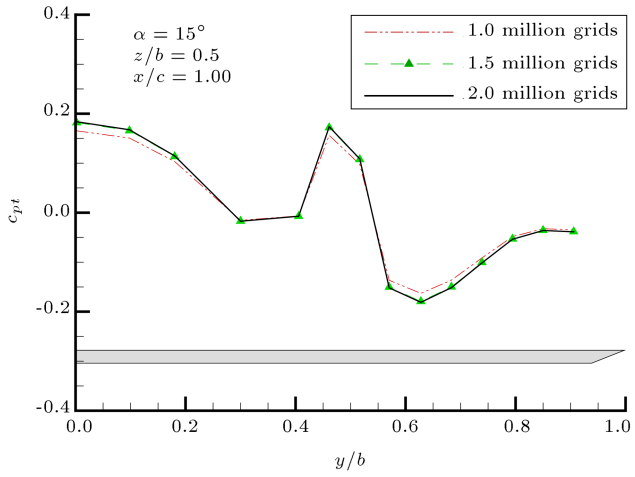

Figure 5. Grid resolution study on the present model.

considered by the authors to check the numerical settings. The lift and drag coefficients have been compared with the Hummel's experimental data. Figure 6(a) and (b) compare the present numerical prediction results with the experimental data [18] and as can be seen, good agreement is achieved. The model considered in the present experiments is somehow similar to that of Hummel's [17], regardless of some geometric details, the free stream conditions and canard deflection angles. Thus nearly the same numerical settings were used to simulate the model constructed for the present experiments.

4. Flowfield description over the model

Figure 7 shows the flowfield obtained by the numerical simulations over the wing in the presence of canard at three chordwise sections for several angles of attack with zero canard deflection.

For $\alpha = 5$ and 15 degrees at $x/c = 0.69$, the canard vortex is clearly observed which seems to be merged with the wing vortex at $x/c = 1$ at the trailing

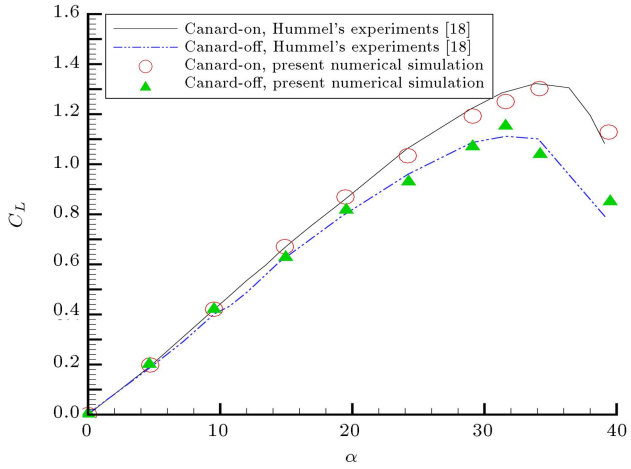

(a) Lift coefficients for canard-on and canard-off cases

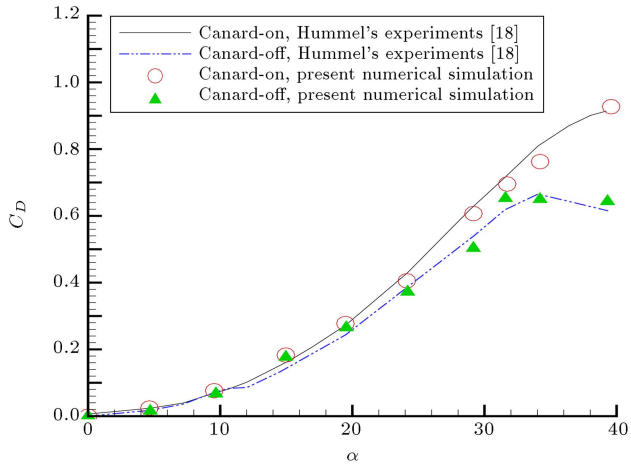

(b) Drag coefficients for canard-on and canard-off cases

Figure 6. Comparison of the present numerical results for a standard canard-wing configuration with the experimental results of Ref. [17].

edge. For $\alpha = 25$ degrees, neither of the three lateral sections on the wing show the individual canard vortex on the wing. It seems that the two vortices have been completely merged and formed a single vortex at the trailing edge.

Similar findings were also documented by Hummel and Oelker [5,6,17]. According to their experimental analysis on a nearly similar canard-wing-body configuration using conical five-hole probe along with balance data and surface pressure measurements, the canard induced up wash along the leading wing edge increases the effective angle of attack in that region. This increase in angle of attack, in turn, supports flow separation at the leading edge. This mechanism is responsible for the growth of the wing vortex along the leading edge [18]. Hummel's results also show that the canard vortex system under the wing influence moves above the wing towards the body and, at the same time, downward towards the wing surface. This trajectory is shown schematically in Figure 8.

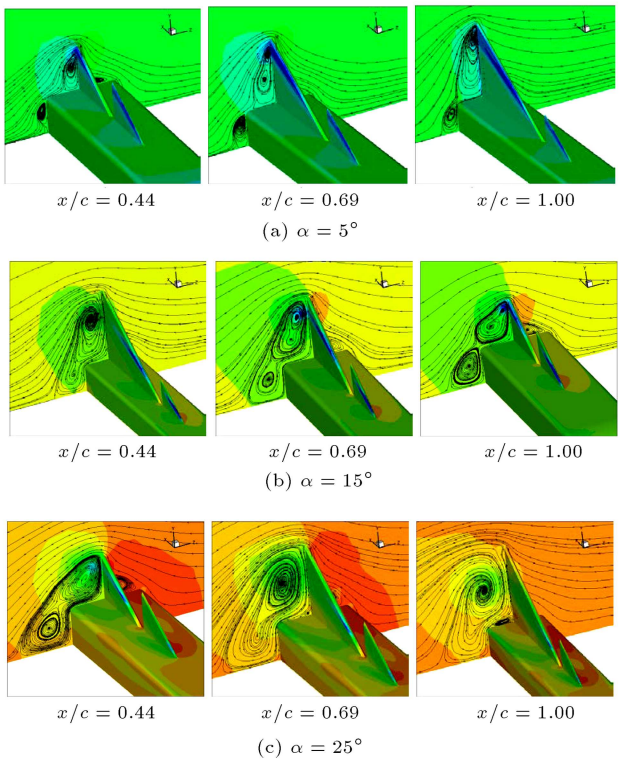

(a) $\alpha = 5°$

(b) $\alpha = 15°$

(c) $\alpha = 25°$

Figure 7. Sectional flowfield on the wing determined by numerical simulations.

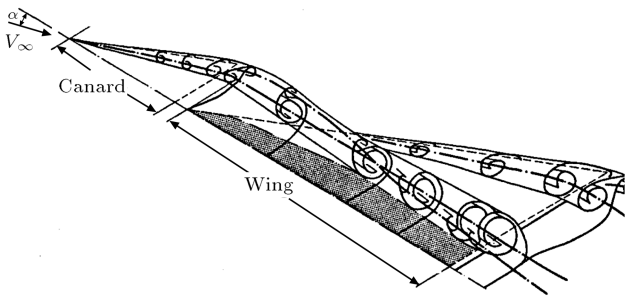

Figure 8. Schematic overview of the vortices on a canard-wing configuration at low angles of attack in the absence of viscous effects [17].

5. Results

The numerical simulation result has been compared with the present experimental data for a typical case in Figure 9. As pointed out earlier, the rake used for these experiments, was not wide enough to cover the entire wing span, thus, the experimental data in this figure were according to the rake width rather than the wing span which was the case for the numerical results. Figure 9 shows a good agreement between the numerical and experimental data. However some discrepancies are observed in this figure which are mostly around the vortex core regions on the wing. These are believed to be due to viscous effects and turbulence modeling used in the numerical simulation and the errors associated with the sensor reading and

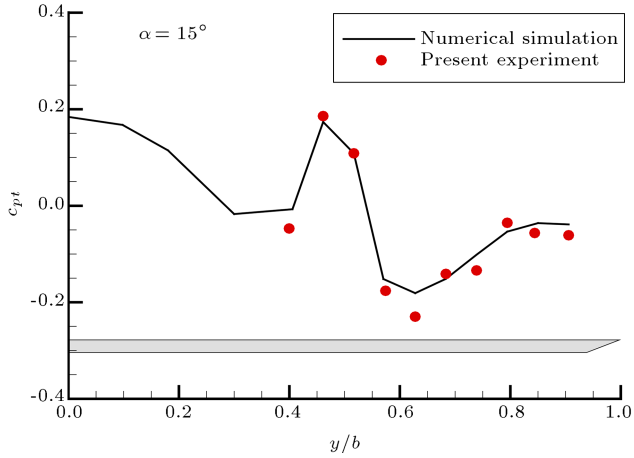

Figure 9. Typical comparison of the present experimental results and the numerical simulations on the model under study.

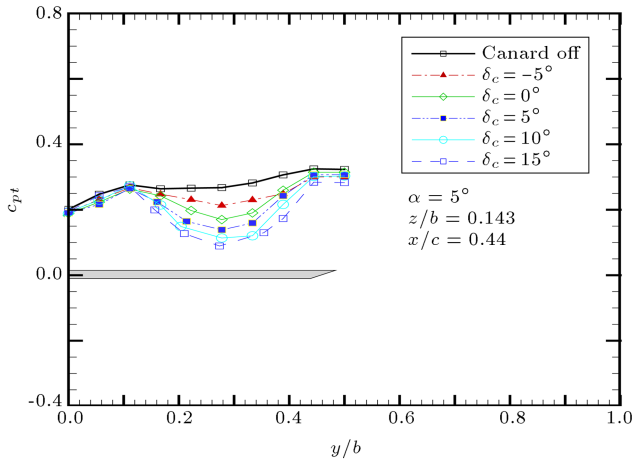

Figure 10. Spanwise velocity distribution; $\alpha = 5°$, $z/b = 0.143$ and $x/c = 0.44$.

the experimental apparatus. The later has been shown in Figure 3.

Figure 10 shows the spanwise variations of the total pressure coefficient for a distance, $z/b = 0.143$, above the wing surface and at a chordwise position of $x/c = 0.44$ at the front half of the wing. For the isolated wing at 5 degrees angle of attack, potential flow dominates and there is no significant variation in the spanwise velocity. However, for the canard-on cases, the spanwise total pressure has been significantly reduced.

For zero deflection angle of canard, even though the flowfield on both the canard and the wing are the same owing to their equal sweep angles, a vortex has been developed over the wing. For a canard deflection of -5° for which the effective canard angle is zero, this vortex becomes weaker. When the canard deflection angle increases to 15°, the angle seen by the canard would be 20° and a strong vortex is appeared on the wing.

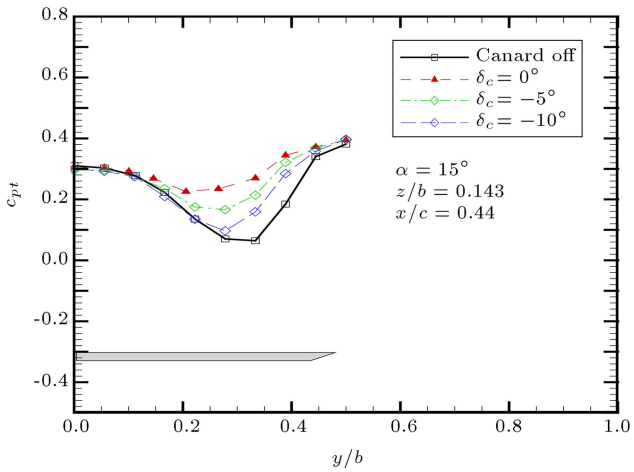

Figure 11. Spanwise velocity distribution; $\alpha = 15°$, $z/b = 0.143$ and $x/c = 0.44$.

Note that at $\alpha = 5°$, no vortex is developed over the isolated wing. Thus the vortex observed over the wing in Figure 10 in the presence of canard is due to the induced effects of canard flow on the wing, which has accelerated the weak flow of the wing to form a relatively strong vortex. Furthermore, from this figure, it can be seen that as the canard angle is increased from -5 to 15 degrees, the width of the low pressure region on the wing also increases, since the canard vortical flow at positive incidence angles affects a wider region on the wing than the negative ones.

Figure 11 shows the spanwise total pressure distribution over the wing for an angle of attack of 15° at a vertical distance, $z/b = 0.143$, from the wing surface. At this angle, the isolated wing vortex has just matured. According to this figure, the wing vortex for zero canard deflection is weaker than that for -5 and -10 degrees deflection. This means that as the canard vortex strength decreases, the strength of the vortex induced on the wing increases. The reduction in total pressure over the model, as seen from Figure 11, may be due to the downwash effect of the canard vortex on the flowfield over the wing at the location under consideration [18]. For the angles well below that corresponding to vortex burst, the canard downwash reduces the effective angle seen by the wing and as a result, the wing vortex strength reduces. For a weaker canard vortex, this downwash effect reduces and evidently the wing vortex strength increases. One may conclude that at a certain canard deflection angle, the combination of the canard and the wing vortices results in a considerable potential flow over the wing, i.e. the viscous effects of the vortex will be diminished.

An interesting phenomenon observed from this figure is that for the chordwise location under consideration, i.e. $x/c = 0.44$, which is at the front half of the wing at $\alpha = 15°$, the vortex on the isolated wing was stronger than that in the presence of canard. This

is believed to be due to the canard downwash effect in the front region of the wing, discussed earlier. For the canard-on cases, it can be inferred that at the front regions of the wing, interaction of a strong wing vortex and a strong canard vortex attenuates the resulting vortex on the wing, while a weak canard vortex induces a favorable effect on a strong wing vortex and improves the wing aerodynamic performance.

The authors' previous findings in an individual study [18,19] revealed that the dominant frequency mode of the canard vortex is higher than that of the wing with the same sweep angle placed downstream. This is due to the canard wake and vortex effects on the wing leading edge vortex, which seems to restrict its activity and decrease its strength. However, at sufficiently high angles of attack, where both the canard and the wing vortices sufficiently grow up, the wing vortex strength cannot be as amplified as that of an isolated wing, due to the retarding effects of the canard vortex.

For 25 degrees angle of attack case, shown in Figure 12, the strong wing vortex, once interacted with a weaker vortex of the canard, is amplified and also moved laterally towards the root; the position which is closer to the canard vortex path on the wing, as illustrated schematically in Figure 8.

In this case, where the canard vortex is weaker than the wing vortex due to different angles of attack seen by either of them, the canard does not play a retarding role on the wing as was the case for the strong canard vortex. In such circumstances, the wing vortex with its lower dominant frequency takes the advantages of the canard higher frequency spectrum to be amplified. As a result, a strong wing vortex downstream of the weak canard vortex would be stronger than that of the wing in the absence of canard, i.e. the isolated wing. From Figure 11, it is also observed that the minimum total pressure on the wing not only reduces, but also moves closer to the junction of the wing and the body. As a consequence of combination of the canard and the wing vortices, the resulting vortex is wider and covers a larger portion of the wing surface, which is observed in Figure 12.

Figure 13 shows the spanwise velocity distribution at a middle section on the wing, $x/c = 0.69$, at 5 degrees angle of attack. It can be seen that the nearly-potential flow over the isolated wing at $\alpha = 5°$ has been replaced by a vortical flow in the canard-on configuration and as the canard deflection angle increases, the vortex strength induced on the wing also increases. As observed earlier, the best aerodynamic performance has been achieved on the wing when the wing weak vortex was interacted with the canard strong vortex, i.e. the wing angle of attack of 5 degrees and the canard effective angle of 20 degrees.

Shown in Figure 14 is the spanwise velocity for section $x/c = 0.69$ at an angle of attack of 15°. The interaction of the strong wing vortex and the strong canard vortex at zero and -5 degrees canard deflection

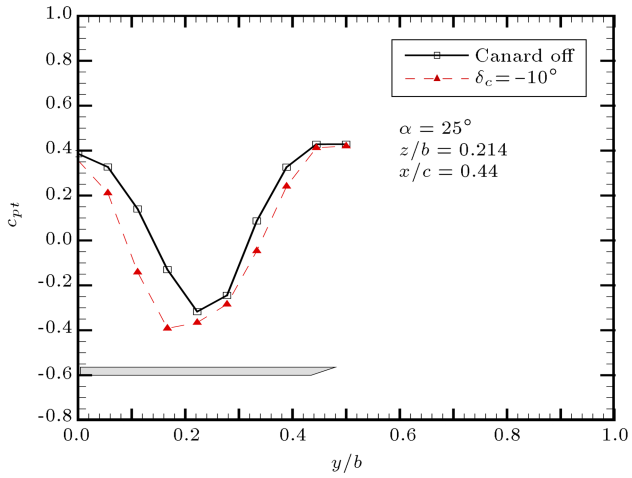

Figure 12. Spanwise velocity distribution; $\alpha = 25°$, $z/b = 0.214$ and $x/c = 0.44$.

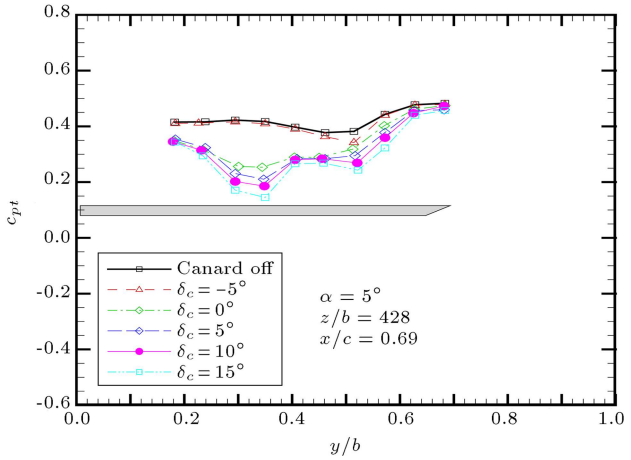

Figure 13. Spanwise velocity distribution; $\alpha = 5°$, $z/b = 0.428$ and $x/c = 0.69$.

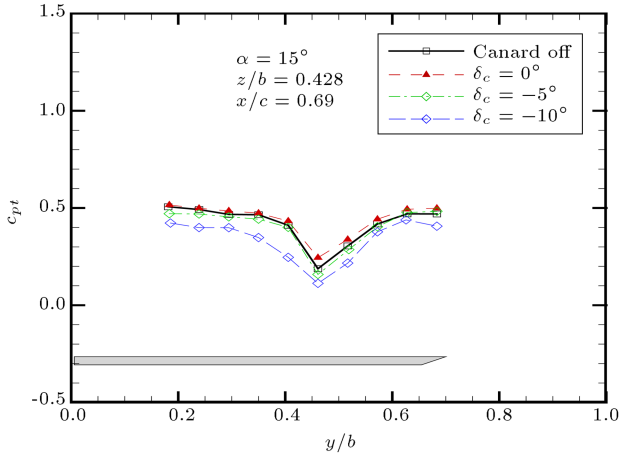

Figure 14. Spanwise velocity distribution; $\alpha = 15°$, $z/b = 0.428$ and $x/c = 0.69$.

has reduced the wing vortex strength in presence of the canard. However, for a weaker vortex developed on the canard for -10° deflection, its interaction with the strong wing vortex could successfully increase the resulting vortex strength on the wing.

In this case, the canard vortex is strong enough to dictate its higher frequency modes to the strong wing vortex with a little lower frequency band [19]. Consequently, the canard shows its destructive effect again and the wing vortex is attenuated in comparison to that of the isolated wing.

In Figure 15, the strong wing vortex at $\alpha = 25°$ has been amplified by the weaker canard vortex at an effective deflection angle of 15°. Once again, the result is a strong vortex, which has been displaced laterally towards the wing root. Further, the vortex on the isolated wing covers less area on the wing than that downstream of the -10° deflected canard.

For the trailing edge section at $x/c = 1.0$ shown in Figure 16, the behavior is similar to that observed in Figure 13 for the middle section. According to Figure 16, the interaction of the wing weak vortex and the canard strong vortical flow at a canard incidence of 15°, corresponding to an effective canard angle of 20°, resulted in a strong vortex on the wing at 5 degrees angle of attack in the presence of canard.

At an angle of attack of 15°, where the wing vortex is matured, Figure 17 shows that the weaker the canard vortex, the stronger would be the wing vortex in the presence of canard. As the canard vortex strength increases, the strength and size of the vortex on the wing decreases. This result has previously been observed at the front and middle sections of the wing.

At 25 degrees angle of attack, where the isolated wing vortex is strong enough, its combination with the weaker vortex of the canard has amplified the wing vortex.

The width of the resulting vortex has also been increased over the wing surface. This situation has been shown in Figure 18.

To have a qualitative view of the flow over the

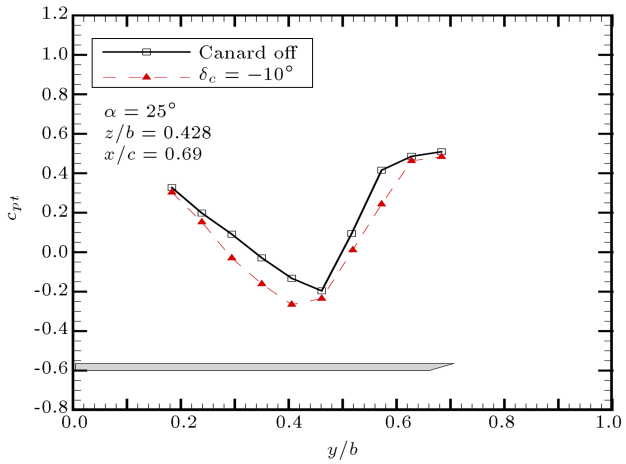

Figure 15. Spanwise velocity distribution; $\alpha = 25°$, $z/b = 0.428$ and $x/c = 0.69$.

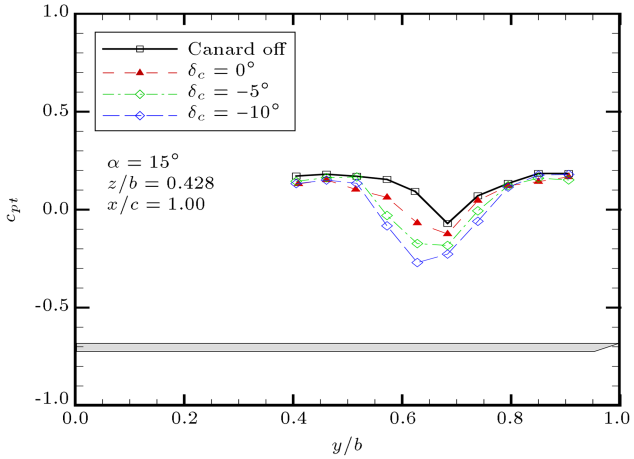

Figure 17. Spanwise velocity distribution; $\alpha = 15°$, $z/b = 0.428$ and $x/c = 1.00$.

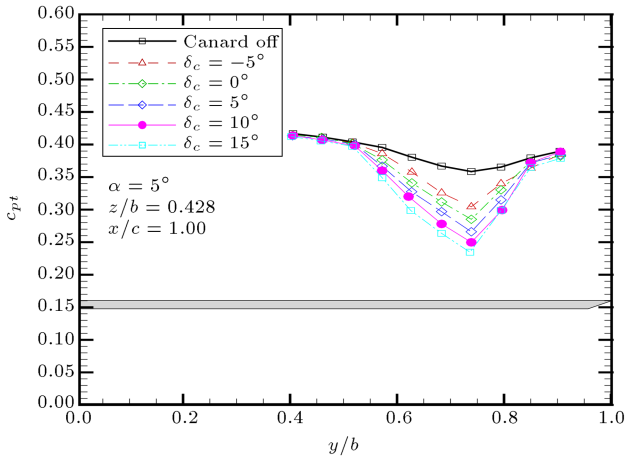

Figure 16. Spanwise velocity distribution; $\alpha = 5°$ $z/b = 0.428$ and $x/c = 1.00$.

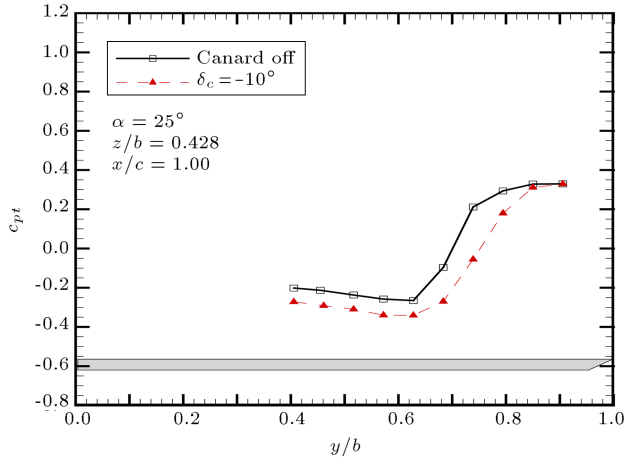

Figure 18. Spanwise velocity distribution; $\alpha = 25°$, $z/b = 0.428$ and $x/c = 1.00$.

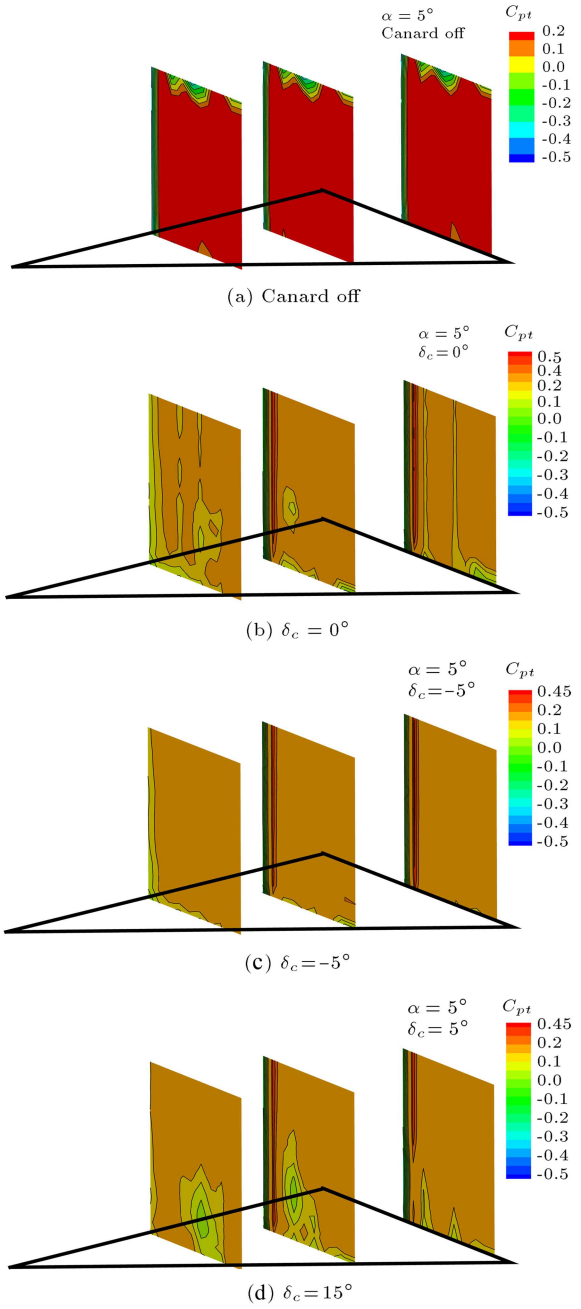

Figure 19. Velocity field on the wing at various canard deflections; $\alpha = 5°$.

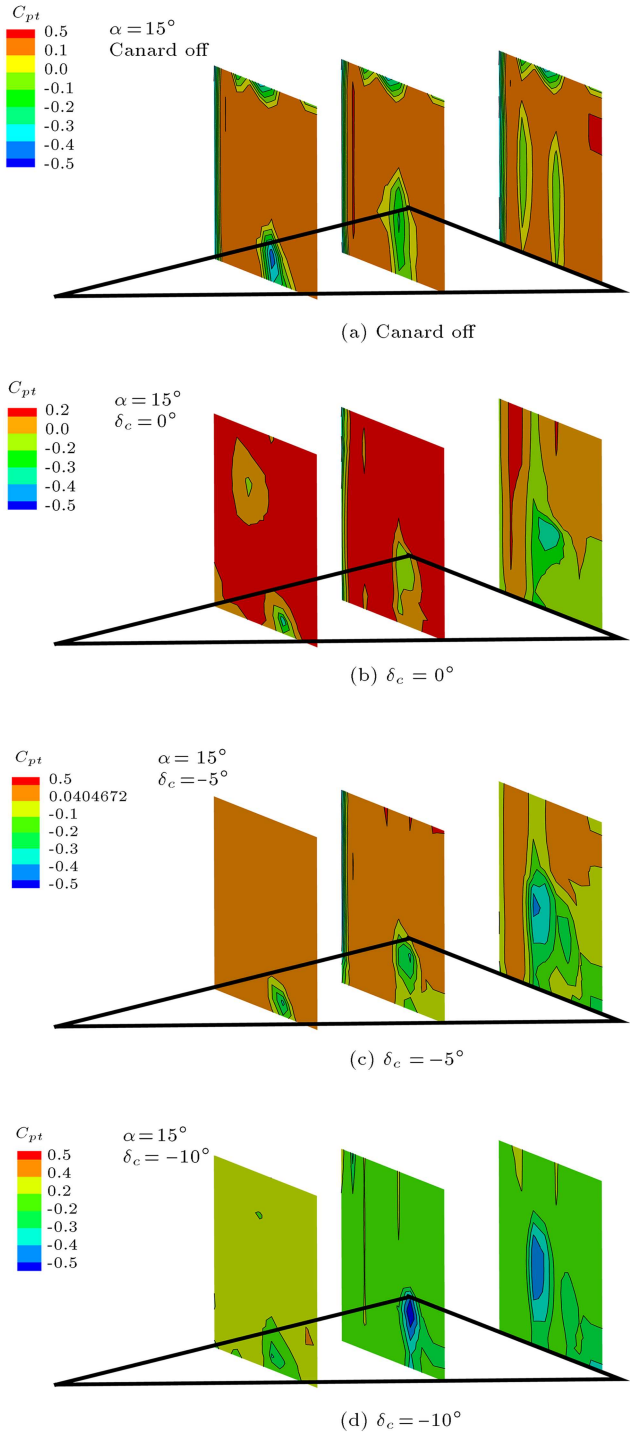

Figure 20. Velocity field on the wing at various canard deflections; $\alpha = 15°$.

wing in the presence of canard, Figures 19, 20 and 21 show the total pressure contours over the wing for canard-off and canard-on cases at various canard deflection angles for three angles of attack of 0, 5 and 15 degrees, respectively. The measurements were on the three aforementioned chordwise sections, $x/c = 0.44$ nearly at the front part, $x/c = 0.69$ at the mid part, and 1.00 at the rear part of the wing.

Figure 19 shows the velocity field on the wing at an angle of attack of 5°. On the isolated wing at this angle of attack, as observed earlier, potential flow dominates throughout the surface as shown in Figure 19(a). For the canard-on configuration at $\delta = 0$, the actual angle seen by the canard is 5°. Even though no vortical flow at this angle exists on the canard nor on the isolated wing, according to Figure 19(b), a vortex can be observed at the front part of the wing as a result of merging the potential flows of both canard and wing. For $\delta = -5°$, the effective canard angle is zero and, as Figure 19(c) shows, the flowfield is similar

to that of an isolated wing. When the canard is set to 15 degrees deflection corresponding to 20° effective angle, a relatively strong vortex is developed on the wing at the front and the middle regions, Figure 19(d). Note that the isolated wing itself has no vortex on its surface at this angle of attack. Thus the vortex seen on the wing in the presence of the canard is the result of amplifying the wing flow by the canard flowfield.

For an angle of attack of 15°, the vortical flow is developed on the isolated wing as shown in Figure 20(a). For zero degrees canard deflection corresponding to an effective angle of attack of 15°, the canard vortex affects the wing vortex of the same strength. The result is a weaker vortex on the wing, Figure 20(b). In Figure 20(c) at $\delta = -5°$, the canard sees 10° deflection angle and a weaker vortex from the canard affects the wing vortex. The adverse effect of canard vortex on the wing is decreased here comparing to Figure 20(b) because the canard vortex strength is reduced. For weaker canard vortex at $\delta = -10°$, shown in Figure 20(d), the wing performance becomes even better than the two former cases with stronger canard vortices.

When the angle of attack is increased to 25° in Figure 21, a strong vortex is dominated on the isolated wing as shown in Figure 21(a). However, though not tested here, this strong vortex could be weakened by the strong canard vortex for zero or positive canard deflections. For $\delta = -10°$ in Figure 21(b), the actual angle seen by the canard is 15° and the canard vortex would be weaker than that of the wing. The result, as observed, is a stronger vortex especially at the rear parts where the isolated wing vortex is about to bust. However, the weaker vortex of canard could successfully revive this vortex at the trailing edge and increase the wing aerodynamic performance.

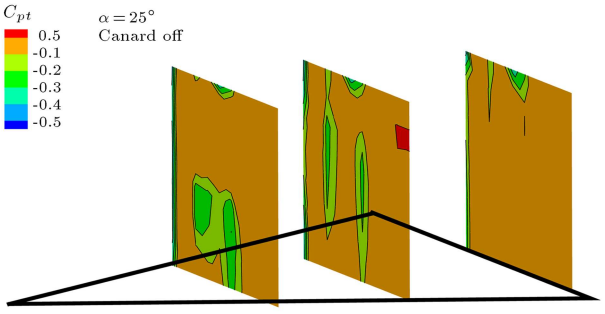

(a) Canard off

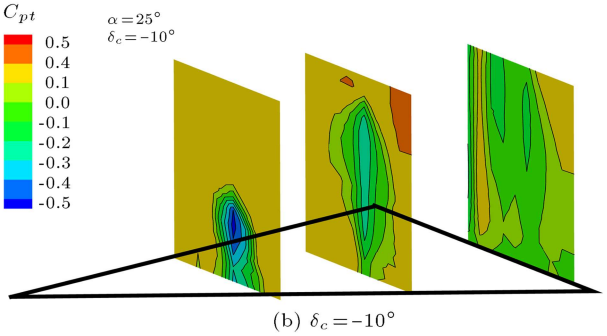

(b) $\delta_c = -10°$

Figure 21. Velocity field on the wing at various canard deflections; $\alpha = 25°$.

6. Concluding remarks

Extensive subsonic wind tunnel tests have been performed on a canard-wing-body configuration to study the canard and wing vortices interaction at various combinations of angle of attack and canard deflection angle. The total pressure distribution at three chordwise sections on the wing in a plane normal to the surface at the section under consideration was measured using a rake. The results, which can be thought as the velocity distribution, show that the wing downstream of canard has a different flowfield than an isolated one. The canard and the wing vortices are shown to have a strong interaction. The canard vortex can either amplify or attenuate the wing vortex, depending on their strengths. According to the results, when the strong vortex of the wing is exposed to the strong vortical flow of the canard, the outcome would be a weaker vortex. As the canard vortex strength decreases, the resulting vortex increases. On the other hand, in the cases where there is a weak or no vortical flow on the wing, the canard vortex can effectively amplify it and a strong vortex is developed on the wing. These results can be generalized to suggest that the merging of two vortices or the induced effect of one vortex on the other, is a function of the vortices strengths. Once the vortices have different strengths, the induced effect or the merging of these vortices results in a stronger vortex, while on the other hand, the merging of two equal strength vortices or the induced effects of either of them on the other may result in a weaker vortex with a smaller size than the two original vortices.

Nomenclature

α	Body angle of attack, measured with respect to the oncoming flow
δ_c	Canard deflection angle, measured with respect to the body
p	Local static pressure
p_t	Local total pressure
c_{pt}	Total pressure coefficient
c	Wing chord at the root
b	Wing semi span

x/c	Nondimensional chordwise position, measured from the wing apex
y/b	Nondimensional spanwise position, measured from the wing root
z/b	Nondimensional vertical position, measured from the wing surface.

References

1. Skow, A.M. "An analysis of the Su-27 flight demonstration at the 1989 Paris air show", *SAE paper*, No. 901001 (April 1990).
2. Er-El, J. "Effect of wing/canard interference on the loading of a delta wing", *Journal of Aircraft*, **25**(1), pp. 18-24 (1987).
3. Calarese, W. "Vortex interaction effects on the lift/drag ratio of close-coupled canard configurations", *AIAA Paper*, pp. 87-1344 (1987).
4. Rom, J., Melamed, B. and Almosnino, D. "Experimental and nonlinear vortex lattice method results for various wing-canard configurations", *Journal of Aircraft*, **30**(2), pp. 207-212, (March-April 1993).
5. Hummel, D. and Oelker, H.C. "Effects of canard position on the aerodynamic characteristics of a close-coupled canard configuration at low speed", AGARD-Cp-465 (1989).
6. Hummel, D. and Oelker, H.C. "Low-speed characteristics for the wing-canard configuration of the international vortex flow experiment", *Journal of Aircraft*, **31**(4), pp. 868-878 (1994).
7. Howard, R.M. and O'Leary, J.F. "Flow field study of a close-coupled canard configuration", *Journal of Aircraft*, **31**(4), pp. 908-914 (July-Aug. 1994).
8. Bergmann. A. and Hummel, D. "Aerodynamic effects of canard position on a wing body configuration in symmetrical flow", *AIAA Aerospace Science Meeting and Exhibit*, 39th Reno, Nevada (Jan. 2001).
9. Eugene, L. Tu "Vortex wing interactions of a close-coupled canard configuration", *Journal of Aircraft*, **31**(2), pp. 314-324 (March-April 1994).
10. Ekaterinaris, J.A. "Analysis of flowfields over missile configurations at subsonic speeds", *Journal of Spacecraft and Rockets*, **32**(3), pp. 385-391 (May-June 1995).
11. Tuncer, I.H. and Platzer, M.F. "A Computational study of a close-coupled delta canard-wing-body configuration", *AIAA Paper 96-2440-CP* (1996).
12. Liu, P., Wen, R. and Zhang, G. "Effects of canard sweep and canard-spanwise blowing magnitude on lift increment", *Journal of Aircraft*, **43**(5), pp. 1369-1371 (September-October 2006).
13. Liu, P., Wen, R., Zhang, G. and Wu, S. "Experimental study of canard-spanwise pulsed blowing on a canard configuration", *Journal of Aircraft*, **45**(5), pp. 1816-1820 (September-October 2008).
14. Cui, Y.D., Lim, T.T. and Tsai, H.M. "Control of vortex breakdown over a delta wing using forebody slot blowing", *AIAA Journal*, **45**(1), pp. 110-117 (2007).
15. Cui, Y.D., Lim, T.T. and Tsai, H.M. "Forebody slot blowing on vortex breakdown and load over a delta wing", *AIAA Journal*, **46**(3), pp. 744-751 (March 2008).
16. Chung, H.S., Seaver, C.A. and McLaughlin, T.E. "Vortex flow control over a delta wing by co-rotating and counter rotating vortex generator", *AIAA Paper 2010-4952* (June-July 2010).
17. Oelker, H.C. and Hummel, D. "Investigations on the vorticity sheets of a close-coupled delta-canard configuration", *Journal of Aircraft*, **26**(7), pp. 657-666 (July 1989).
18. Soltani, M.R., Askari, F., Davari, A.R. and Nayebzade, A. "Effects of canard position on the wing surface pressure", *International Journal of Science and Technology, Scientia Iranica, Transactions B: Mechanical Engineering*, **17**(2), pp. 102-107 (March-April 2010).
19. Samimi, S., Davari, A.R. and Soltani, M.R. "Canard-wing interactions in subsonic flow", *International Journal of Science and Technology, Transactions of Mechanical Engineering*, **37**(M2), pp. 133-147 (2013).

Biographies

Ali Reza Davari received his PhD degree in Aerospace Engineering from Sharif University of Technology, Tehran, Iran, in 2006, and is currently faculty member in the Department of Mechanical and Aerospace Engineering at the Science and Research Branch, Azad University, Iran. His research interests encompass experimental and applied aerodynamics, including new prediction and optimization methods and tools in aerodynamics, such as neural networks, DOE/RSM and evolutionary algorithms.

Mostafa HadiDoolabi has been graduated in 2006 with a PhD degree in Aerospace Engineering from Amirkabir University of Technology, Tehran. He is currently a faculty member in the Department of Aerospace Engineering at Malek Ashatr University. His main areas of study are numerical aerodynamics and flight mechanics. He is specially interested in the numerical schemes development for unsteady and high speed flows. Wind tunnel design, calibration and tests have been his recent research areas.

Mohammad Reza Soltani obtained his PhD de-

gree in Aerodynamics from the University of Illinois at Urbana-Champaign, USA, in 1991, and is currently Professor in the Aerospace Engineering Department at Sharif University of Technology, Tehran, Iran. His research interests include unsteady and applied aerodynamics, design and building of wind tunnels and wind turbines, design, building and implementation of wind tunnel instruments, and measurement methods. He has published over 27 journals and 50 conference papers in his areas of research.

Mohammad Izadkhah received his MSc degree in aerospace engineering from Sharif University of Technology. Wind tunnel test has been his primary research interest and he has good experiences in low speed wind tunnel tests, especially wing-body interaction problems in subsonic flow.